Cell Host & Microbe, Volume *9*

Supplemental Information

Structural and Functional Analysis of a Plant Resistance Protein TIR Domain Reveals Interfaces for Self-Association, Signaling, and Autoregulation

Maud Bernoux, Thomas Ve, Simon Williams, Christopher Warren, Danny Hatters, Eugene Valkov, Xiaoxiao Zhang, Jeffrey G. Ellis, Bostjan Kobe, and Peter N. Dodds

INVENTORY OF SUPPLEMENTAL INFORMATION

Supplemental information contains seven supplemental figures, two supplemental tables and one supplemental experimental procedure table.

Supplemental figures:
Figure S1, related to Figure 1
Figure S2, related to Figure 2
Figure S3, related to Figure 3
Figure S4, related to Table 1
Figure S5, related to Figure 4
Figure S6, extended data from Figure 4

Supplemental tables:
Table S1, related to Figure 2D
Table S2, related to Table 1

Supplemental experimental procedures:
Table: Primers sequences used to generate Gateway L6 constructs

SUPPLEMENTAL INFORMATIONS

SUPPLEMENTAL FIGURE AND TABLE LEGENDS

SUPPLEMENTAL FIGURES

Figure S1. Mutations in L6 TIR domain affect HR induction and signalling activation but not effector recognition. (A) Overexpression of TIR domains from different L alleles triggers cell death. Flax Hosh plants 12 days after infiltration with *A. tumefaciens* strains carrying L allele (L6, L10, L7, L2) TIR_{1-248} constructs. (B-D) Western blot analysis of L6 TIR domain mutants. Protein expression of full-length L6 with mutations in the TIR domain 7 days after agroinfiltration in tobacco leaves (A) or in yeast cells coexpressing AvrL567 GAL4-BD fusion (B). Proteins were detected with anti-HA antibodies. (C) Protein expression of $L6_{1-248}$ mutants fused to YFP 3 days after agroinfiltration in flax leaves. Proteins were detected with anti-GFP antibodies.

Figure S2. Crystal structure of L6 TIR domain. (A) Superposition of L6TIR (red) with the AtTIR structure (green; PDB ID 3JRN). (B) As in A, with the molecules rotated 90° around the y-axis. (C) Superposition of L6TIR (red) with the human TLR2 TIR domain (Xu et al. 2000) (blue; PDB ID 1FYW) in the same orientation as in B.

Figure S3. Sedimentation equilibrium analytical ultracentrifugation. L6TIR protein was analyzed at 0.5 mg/mL in 10 mM Hepes pH 7.4, 150 mM NaCl and two different speeds. The data fitted best to a monomer-dimer model resulting in a dimerization K_d of 20.3 μM. Monte Carlo analysis (1000 iterations with a confidence level of 0.68) gave K_d limits between 18.7 and 21.9 μM.

Figure S4. Mutation analysis of L6 TIR domain. (A) Flax Hosh plants 12 days after infiltration with *A. tumefaciens* strains carrying L6 TIR_{1-233} mutants fused to YFP. (B) Expression of L6 TIR_{1-233} mutants fused to YFP 3 days after agroinfiltration in flax leaves. Proteins were detected with anti-GFP antibodies. (C) Growth of yeast cells co-expressing GAL4-BD and GAL4-AD fused to L6 TIR_{29-233} mutants on synthetic media lacking tryptohane and leucine (-HT) or selective media additionally lacking histidine (-HTL). (D) Expression of L6 TIR_{29-233} constructs fused to GAL4-AD and GAL4-BD. Proteins were detected with anti-HA and anti-Myc antibodies, respectively. (E) MALLS analysis of wild-type L6TIR and of the W131A, R164A, D208A, K200E, K216E and P160Y mutants. The red lines indicate the trace from the refractive index detector, and the blue lines are the weight-average molecular weight distribution across the peak. For each sample the initial protein concentration was

0.5 mg/ml and the buffer consisted of 10 mM Hepes pH 7.4 and 150 mM NaCl. (F) Sedimentation equilibrium AUC analysis of the W131A, R164A, D208A, K200E, K216E and P160Y mutants. All samples were analyzed at 0.5 mg/mL in 10 mM Hepes pH 7.4, 150 mM NaCl and two different speeds. The data for each mutant fitted best to a monomer-dimer model.

Figure S5. Self-association and autoactivity of L10 TIR. (A) Growth of yeast cells co-expressing GAL4-BD and GAL4-AD fused to L10 TIR_{29-233} wt or E216K mutant on synthetic media lacking tryptohane and leucine (-HT) or selective media additionally lacking histidine (-HTL). GAL4-AD and BD proteins fusions were detected with anti-HA and anti-Myc antibodies, respectively. (B) Flax Hosh plants 12 days after infiltration with *A. tumefaciens* strains carrying L10 TIR_{1-233} wt and E216K mutant fused to YFP. Proteins were detected with anti-GFP antibodies.

Figure S6. Comparative analysis of plant TIR domains. (A-D) Conserved regions in plant TIR domains. (A-B) Ribbon diagram of L6TIR colored by sequence conservation calculated using ConSurf (Ashkenazy et al. 2010). The multiple sequence alignment used by ConSurf consisted of 258 unique plant TIR domain sequences with sequence identities to L6TIR ranging from 25-90%. Cyan color corresponds to variable regions, while purple color corresponds to conserved regions. In A, the cross-section of interface 1 is highlighted and the orientation is related to the green molecule in Figure 5A by 90° rotations around both the x and y-axis. The cross-section of interface 2 is shown in B and is related to the yellow molecule in Figure 5A by 90°and 45° rotations around the y and z axis, respectively. In both representations, the residues involved in the interfaces are shown in wireframe. (C-D) Surface representation of the molecules in A and B coloured by decreasing sequence conservation (purple-white-cyan). The positions of conserved surface residues in these regions are labelled. (E-J) Comparative analysis of L6, N and RPS4 TIR domain mutants. Homology models of the RPS4 and N TIR domains where built based on the structure of L6TIR using Modeller (Eswar et al. 2006). Mutational data (Dinesh-Kumar et al. 2000; Mestre and Baulcombe 2006; Swiderski et al. 2009) were mapped onto the structures. Mutants resulting in loss and gain of function are coloured in blue and orange, respectively. (E-G) shows the positions of the mutants in L6 (yellow), RPS4 (light blue) and N (green) relative to interface 2 in L6TIR, while (H-J) shows the positions relative to interface 1.

Figure S7. Western blot analysis of L6 and L7 truncated constructs. (A) Expression of L6 truncated constructs fused to YFP 3 days after agroinfiltration in flax leaves. Proteins were detected with anti-GFP antibodies. The amido black staining of the membrane indicates the level of protein loaded with Rubisco as a reference. (B-C) Expression of truncated L6 (B) and L7 (C) constructs fused to GAL4-BD and GAL4-AD in yeast. Proteins were detected with anti-Myc anti-HA antibodies, respectively. Protein membranes were exposed for 1 or 30 minutes (left and right panel respectively).

Full-length L6 constructs fused to YFP and to GAL4-BD were detected after 30 minutes exposure only.

SUPPLEMENTAL TABLES

Table S1. Crystallographic data and refinement statistics for L6TIR domain

Table S2. Summary of the MALLS and AUC mutant analysis

SUPPLEMENTAL EXPERIMENTAL PROCEDURES

Primer sequences used to generate Gateway L6 constructs. (Table)

Supplemental figures

Figure S1, related to Figure 1

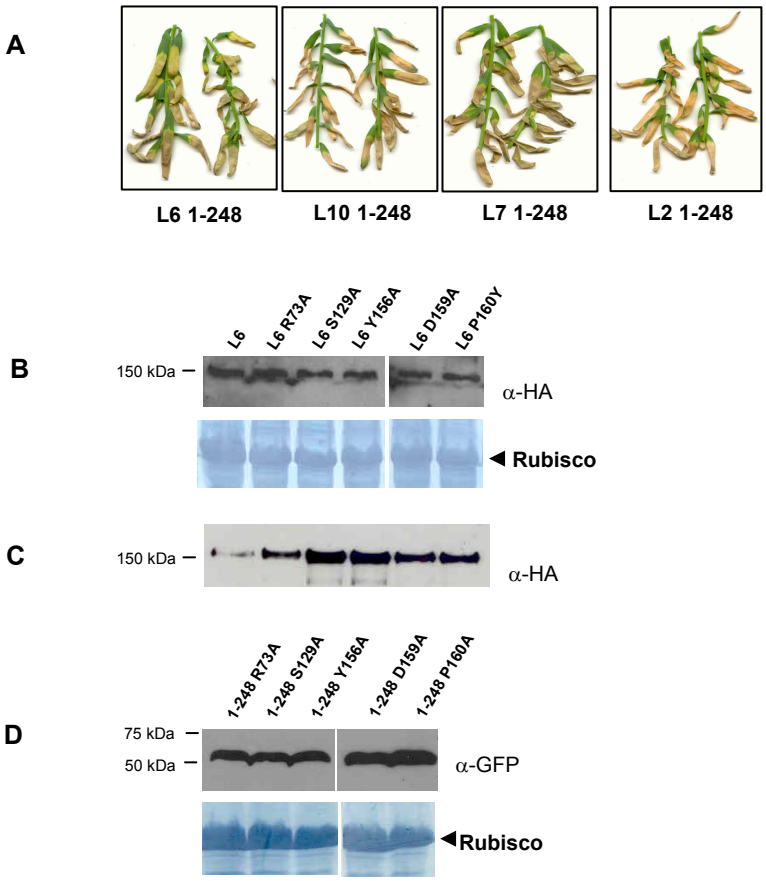

Figure S2, related to Figure 2

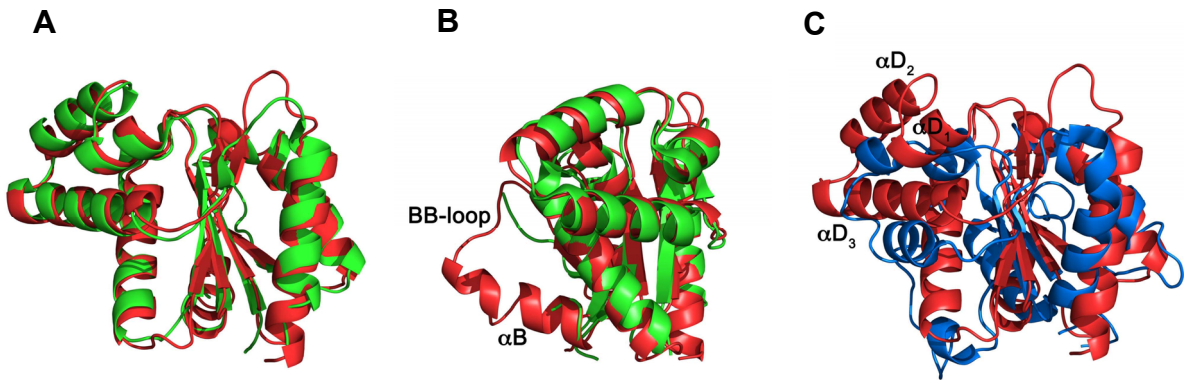

Figure S3, related to Figure 3

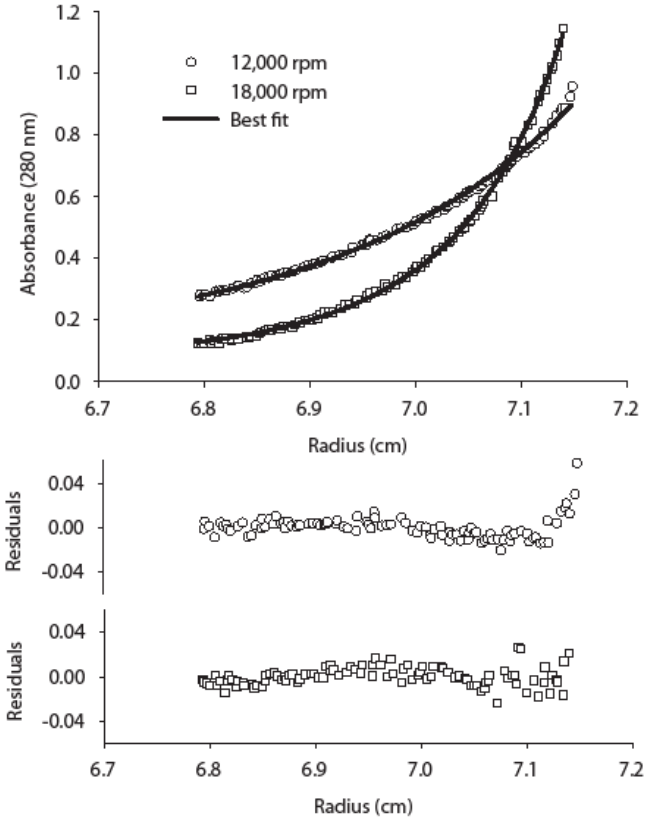

Figure S4, related to Table1

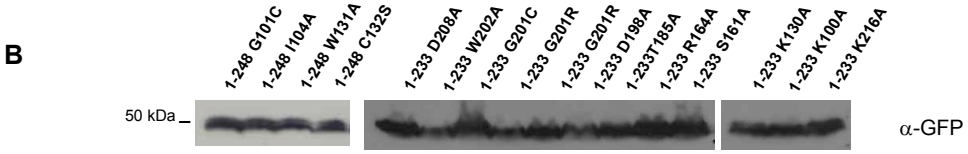

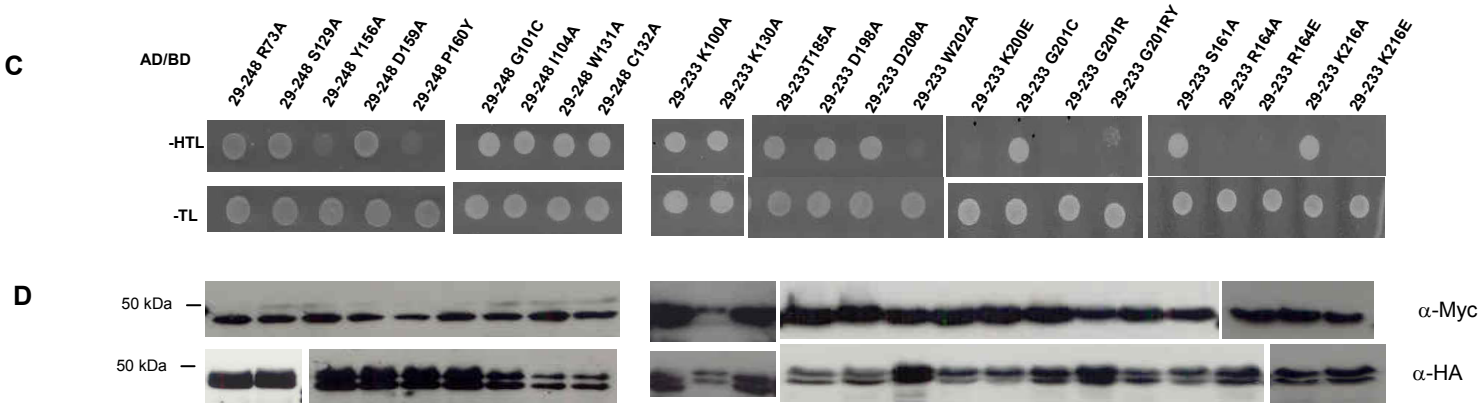

E

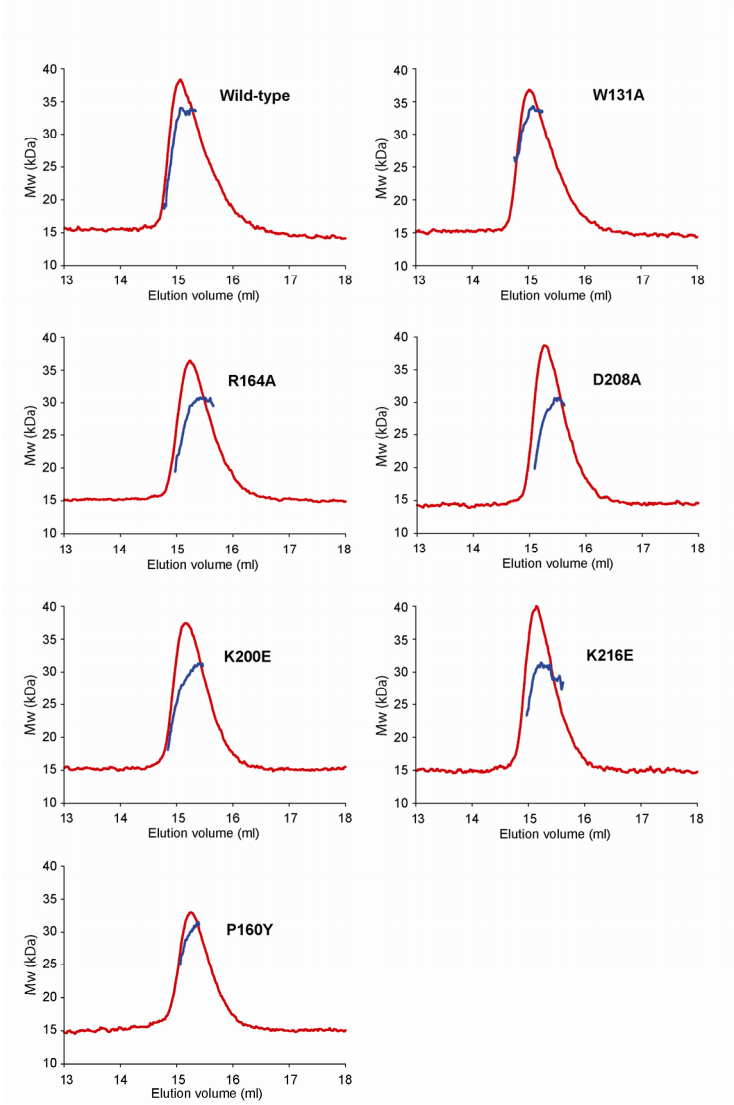
Wild-type
W131A
R164A
D208A
K200E
K216E
P160Y
Mw (kDa)
Elution volume (ml)

F

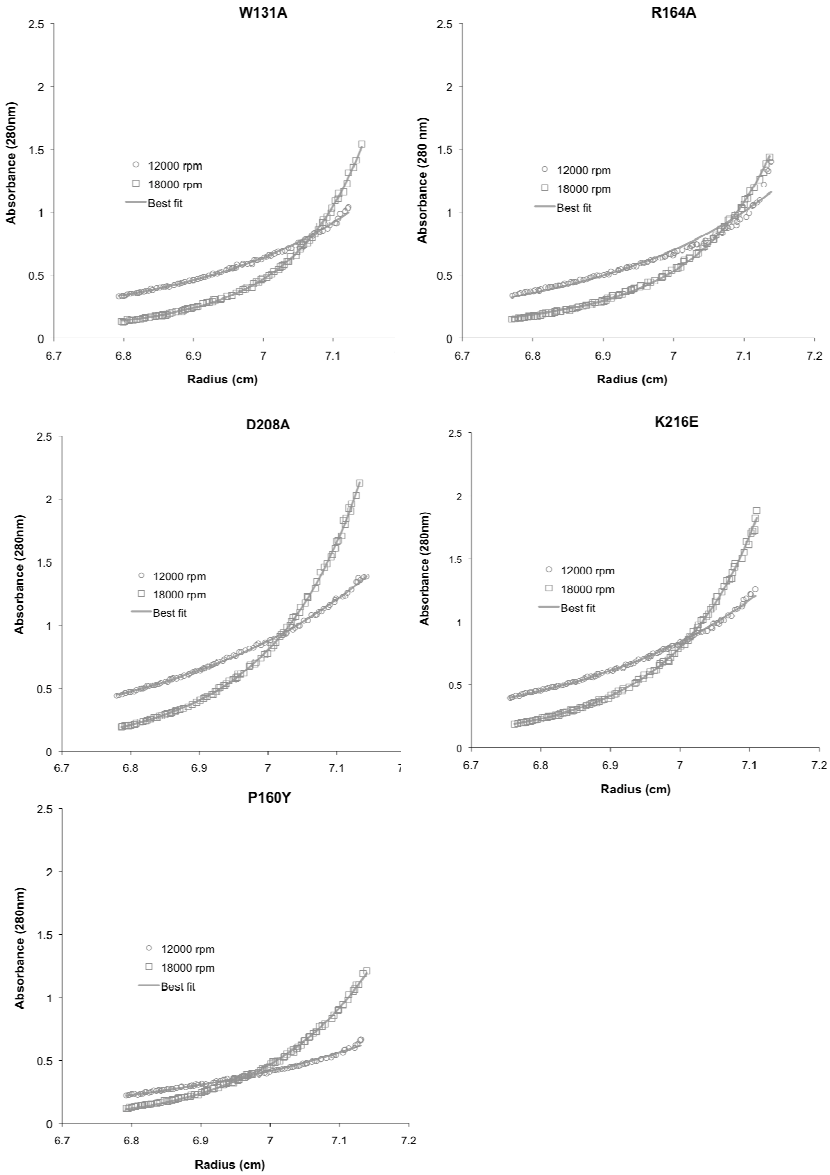
W131A
R164A
D208A
K216E
P160Y
12000 rpm
18000 rpm
Best fit
Absorbance (280nm)
Absorbance (280 nm)
Radius (cm)

Figure S5, related to Figure 4

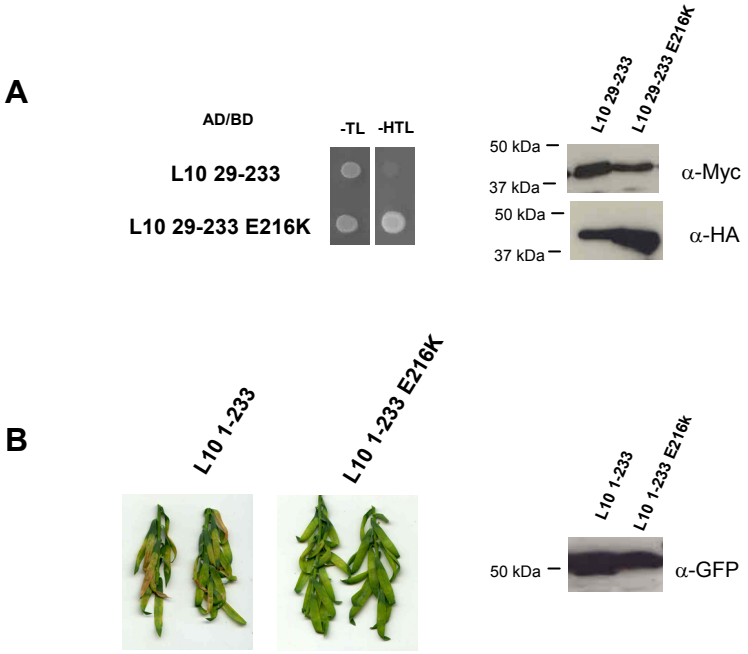

Figure S6, extended data from Figure 4

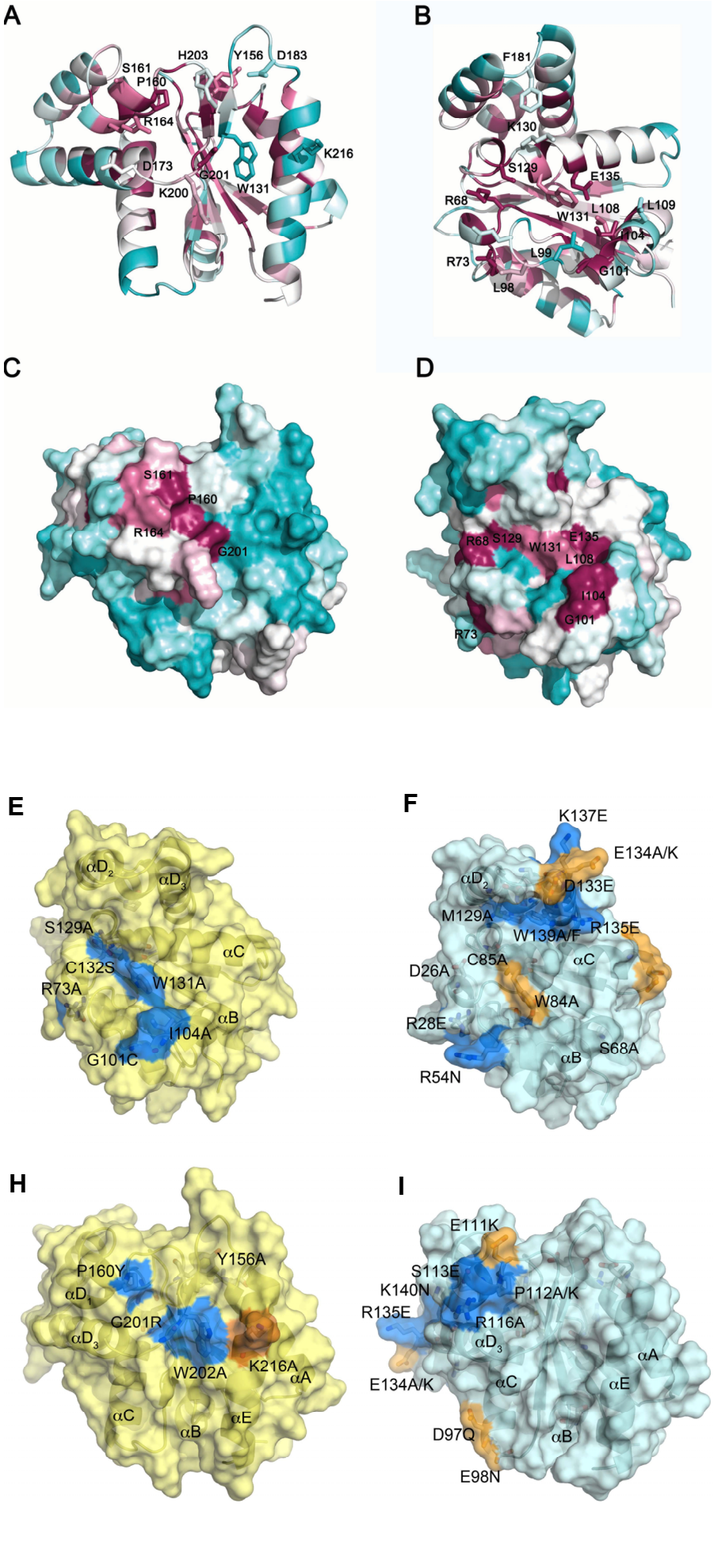

Figure S7, related to Figure 5

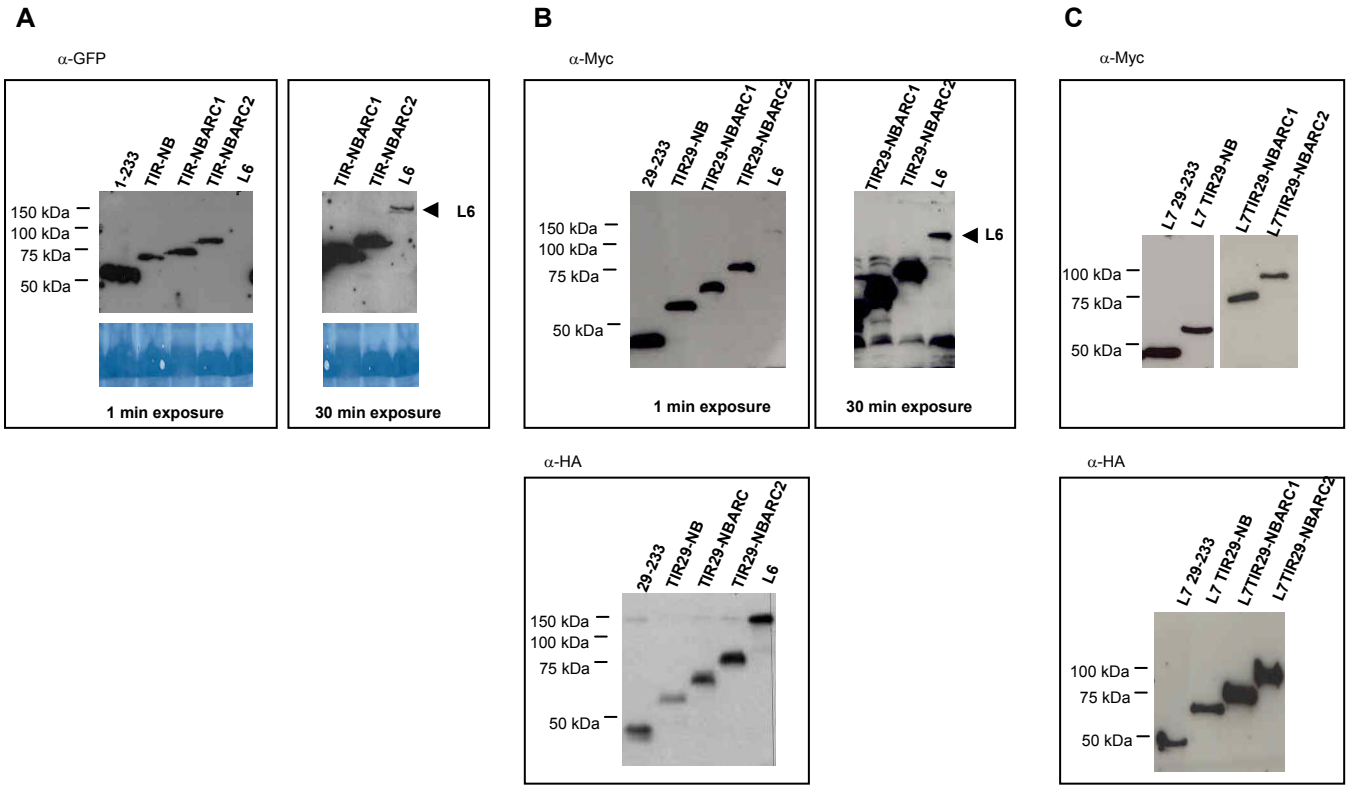

Supplemental tables

Diffraction data statistics	
Space group	$P2_12_12$
Unit cell dimensions (Å)	a=65.9
	b=102.2
	c=58.3
Molecules per asymmetric unit	2
Resolution range (Å)	19.5-2.3 (2.42-2.30)[a]
No. of unique observations	18088
Completeness (%)	99.7 (99.8)
Multiplicity	7.2 (7.0)
R_{merge} (%)[b]	9.3 (32.1)
Average I/σ(I) (%)	16.7 (6.7)
Refinement statistics	
Resolution (Å)	19.3-2.3
No. of reflections work set	17114
No. of reflections test set	918
R_{work} [c] (%)	17.4
R_{free} [d] (%)	23.0
No. of protein atoms	2797
No. of water molecules	183
Overall B factor (Å^2)	23.9
R.m.s deviations from ideal values	
Bonds (Å)	0.008
Angles (°)	1.001
Ramachadran plot (%)	
Favoured	96.4
Disallowed	0

[a] Numbers in parenthesis are for the highest resolution shell.

[b] $R_{merge} = \sum_{hkl}(\sum_i(|I_{hkl,i}-\langle I_{hkl}\rangle|))/\sum_{hkl,i}\langle I_{hkl}\rangle$, where $I_{hkl,i}$ is the intensity of an individual measurement of the reflection with Miller indices h, k and l, and $\langle I_{hkl}\rangle$ is the mean intensity of that reflection. Calculated for $I > -3\sigma(I)$.

[c] $R_{work} = \sum_{hkl}(||Fobs_{hkl}|-|Fcalc_{hkl}||)/|Fobs_{hkl}|$, where $|Fobs_{hkl}|$ and $|Fcalc_{hkl}|$ are the observed and calculated structure factor amplitudes.

[d] R_{free} is equivalent to R_{work} but calculated with reflections (5 %) omitted from the refinement process.

Table S1, related to Figure 2D

	Molecular mass (kDa) by MALLS[a]	Dissociation constant (Kd) by AUC[b] (μM)
Wild-type[1]	35.5	20.3 (22.0 -18.8)
Wild-type[2]	33.9 +/- 0.7	-
W131A	33.8 +/- 1.5	50.5 (54.3 - 46.9)
D208A	27.8 +/- 0.6	337.3 (372.9 - 305.1)
R164A	29.5 +/- 0.5	187.6 (204.5 - 172.1)
K200E	29.1 +/- 0.7	-
K216E	30.4 +/- 0.7	147.5 (160.4 - 135.6)
P160Y	30.3 +/- 0.8	380.6 (432.0 - 335.3)

[a] Average molecular mass at the refractive index peak determined using multi angle laser light scattering (MALLS).

[b] Dissociation constant for dimerisation estimated by analytical ultracentrifugation (AUC) equilibrium sedimentation studies. The values in brackets refer to the 68 % confidence intervals determined by Monte Carlo analysis.

Wild-type 1 (Figure 3) and 2 (Figure S8) are from two different protein batches and were analyzed using different buffer preparations. The mutants were analyzed by MALLS and AUC using the same buffer preparation as for wild-type 2.

Table S2, related to Table 1

Supplemental experimental procedures

Forward primers	primer sequence 5'-3'
AttB1 L6 ATG	CAAAAAAGCAGGCTTAATGAGTTATTTGAGAGAAGTTGCT
AttB1 L6 TIR29	CAAAAAAGCAGGCTTAATGAAAGACTCAATCGTCAACGATGA
AttB1 L6 TIR114	CAAAAAAGCAGGCTTAATGCAGTCCAAAATTTACGTCCCGA

Reverse primers	primer sequence 5'-3'
AttB2 L6 TIR209	CAAGAAAGCTGGGTCCTTGTCATTCTTTCCGATGTGCCA
AttB2 L6 TIR220	CAAGAAAGCTGGGTCATCTGCTGATACTTTGTCTGCT
AttB2 L6 TIR233	CAAGAAAGCTGGGTCTTCTAAAATGAGATTTTCCTTGCT
AttB2 L6 TIR248	CAAGAAAGCTGGGTCTAATACGGCTGTTATGTGATCATCA
AttB2 L6 NB	CAAGAAAGCTGGGTCTTGATTCTCATTCAAAGTACCCA
AttB2 L6 ARC1	CAAGAAAGCTGGGTCACGTAATTGTTCCAACGT
AttB2 L6 NBARC	CAAGAAAGCTGGGTCACATTCGCTCTTAAACTCA
AttB2 L6 end	CAAGAAAGCTGGGTCTCTGTAGGGCTGATCGGGCCATGT

Primers sequences used to generate Gateway L6 constructs